Digital Predistortion of 5G Massive MIMO Wireless Transmitters Based on Indirect Identification of Power Amplifier Behavior With OTA Tests

Xiaoyu Wang, *Student Member, IEEE*, Yue Li, *Student Member, IEEE*, Chao Yu, *Member, IEEE*, Wei Hong, *Fellow, IEEE*, and Anding Zhu, *Senior Member, IEEE*

***Abstract*— In this article, we present a novel digital predistortion (DPD) architecture for multiple-input–multiple-output (MIMO) transmitters using a real-time single-channel over-the-air (OTA) data acquisition loop. The proposed feedback data acquisition strategy captures OTA signals from a fixed location and indirectly identifies the nonlinear behavior of all power amplifiers (PAs) in the array, as well as their combined signals in the far-field direction. The DPD can, therefore, be effectively constructed without direct measurement at PA output or at user end. The proposed linearization solution can run in real-time and, thus, does not interfere with data transmission in the MIMO transmitters. It can also achieve robust performance when mutual coupling occurs between antenna elements. Simulation and experimental results demonstrate that the proposed scheme can accurately estimate both PA outputs and far-field main beam data. Excellent linearization performance can be achieved with low complexity hardware implementation and reduced computational complexity.**

***Index Terms*— Beamforming, digital predistortion (DPD), 5G, millimeter wave, multiple-input multiple-output (MIMO), over-the-air (OTA), power amplifier (PA).**

I. Introduction

TO ACHIEVE higher system capacity, millimeter-wave (mmWave) massive multiple-input multiple-output (MIMO), featuring wide bandwidth and large number of antennas, is expected to be adopted in 5G communication systems [1]. The very short wavelength of mmWave frequencies is beneficial for massive MIMO, as the physical size of antenna can be reduced significantly and considerable performance improvement can be achieved by using large-scale antenna arrays. However, similar to lower frequencies, designing power amplifiers (PAs) at such high frequencies also faces severe challenges because it is not only difficult to maintain both linearity and efficiency at mmWave but also the crosstalk and integration issues in large arrays probably make the design more complicated. On one hand, the complex behavior of PAs and crosstalk between radio frequency (RF) chains require more powerful distortion mitigation methods. On the other hand, the large number of RF chains in the massive MIMO system puts serious constraints on hardware complexity and the related power consumption. Thus, effective yet realistic linearization techniques are desirable.

Digital predistortion (DPD) is one of the most popular PA linearization techniques in modern communication systems [2], [3]. Within the context of MIMO DPD, many DPD models have been proposed to tackle the nonlinearity and crosstalk induced by PAs [4]. In general, these behavioral models can cancel MIMO crosstalk by adding specific cross terms into the model structure [5]–[7]. Nonlinearity caused by mutual coupling effect between different antenna elements was also considered in recent works [8]–[10]. The hardware complexity of such systems is usually very high as they use separate DPD models for each PA. They are also only suitable for fully digital beamforming systems where the digital baseband chain is available for each RF chain. In hybrid beamforming, it is not feasible to use separate DPDs for each PA. Some compromising solutions have been proposed. Reference [11] employed one DPD for each subarray, which minimized average error between the input and output signals of all PAs. The concept of beam-oriented linearization was proposed in [12]–[14]. The target of linearization was the main beam over-the-air (OTA) signals rather than the output of each PA. In this case, the far-field main beam signals can be linearized, but distortions in other directions are not well compensated.

To extract DPD coefficients, a feedback data acquisition path is required. In single-input single-output (SISO) communication systems, there is only one PA in each transmitter, and thus, the PA output signal is usually acquired directly from the output of the PA with a coupler. In massive MIMO systems, the number of RF chains can reach several hundred. Using dedicated feedback paths for each PA separately is not feasible because it will dramatically increase the system implementation complexity. Choi and Jeong [15] proposed a DPD method based on combined feedback, which added

Manuscript received June 17, 2019; revised August 26, 2019; accepted September 14, 2019. Date of publication November 7, 2019; date of current version January 13, 2020. This work was supported in part by the Science Foundation Ireland (SFI) and the European Regional Development Fund under Grant 17/NSFC/4850 and Grant 13/RC/2077 and in part by the National Natural Science Foundation of China (NSFC) under Grant 61861136002. This article is an expanded version from the IEEE International Wireless Symposium, Guangzhou, China, May 19-22, 2019. *(Corresponding author: Xiaoyu Wang.)*

X. Wang, Y. Li, and A. Zhu are with the School of Electrical and Electronic Engineering, University College Dublin, Dublin 4, D04 V1W8 Ireland (e-mail: xiaoyu.wang1@ucdconnect.ie; yue.li1@ucdconnect.ie; anding.zhu@ucd.ie).

C. Yu and W. Hong are with the State Key Laboratory of Millimeter Waves, Southeast University, Nanjing 210096, China (e-mail: chao.yu@seu.edu.cn; weihong@seu.edu.cn).

Color versions of one or more of the figures in this article are available online at http://ieeexplore.ieee.org.

Digital Object Identifier 10.1109/TMTT.2019.2944828

all the PAs' outputs to form single feedback. A single-PA-feedback DPD method in [16] constructs a DPD model for only one PA and uses this model, as all PAs' DPD models in the array. Reference [13] proposed to capture the output of different PAs in a time-division manner so that all PAs can share one feedback receiver. Reference [17] put forward a DPD scheme linearizing all PAs in the transmitter with received signals measured over the air by a few observation receivers. Despite numerous efforts devoted to this field, some critical architecture issues persist. In particular, the use of bulky couplers and the large number of dedicated feedback paths are becoming serious obstacles in the integration of larger arrays.

Another issue that has long been neglected to date is the real-time requirement of MIMO DPD systems. In real operation, MIMO DPD systems must have the following two features: 1) support continuous data transmission and 2) support beam steering. The first requirement implies that DPD calibration cannot interrupt data transmission, and the transmitters in actual base stations do not send repeated data sequences. Thus, for time-shared feedback strategies, such as [13], if output data of each PA are captured one after another, they must come from different input sequences. Since the captured data blocks from different PAs cannot be synchronized or combined, such algorithms are not suitable for real-time mobile communication systems. The second requirement affects the DPD approaches based on beam-oriented linearization or OTA data acquisition. In [12] and [13], all PAs in the array, together with precoder, beamformer, and channel effect, are modeled by a single behavioral model, making the coefficients dependent on the beam direction. As a result, when the beam steers to a different direction, the DPD coefficients need to change accordingly. Therefore, model extraction should either execute fast enough to track the beam change or precalculate the coefficients at all directions. Some DPD methods based on OTA data acquisition also suffer from similar problems. For example, [18] and [19] directly linearize signals received by an observation antenna. However, signals received from different directions generally differ in nonlinear characteristics; these schemes are, therefore, valid only if the DPD antenna happens to be in the same direction as that of the user end.

In this article, we propose a novel MIMO DPD architecture based on a real-time single-channel OTA feedback scheme that can be used to identify PA behavior without direct measurements at PA outputs. In the proposed scheme, an external observation path is equipped to receive the feedback signal at a fixed location near the main transmitter. Due to user movements, the data blocks received at the DPD antenna carry time-varying phase information so that they can be used to identify behavioral models of PAs and to extract DPD model coefficients. In our architecture, bulky couplers are eliminated from the feedback path, and only one feedback receiver is required for the whole array. Moreover, our proposed method is suitable for real-time operation, as continuous data transmission and beam steering are both supported. Beyond our earlier publication [20], this article presents a comprehensive theoretical analysis of the proposed solution and explains how it can be feasibly implemented in a real system. It also includes simplified forward modeling algorithms, theoretical analysis of mutual coupling effect in the signal reconstruction algorithm, and the application of our method to full-angle MIMO DPD systems [21]. Practical considerations, as well as more extensive simulation and experimental results, are also presented.

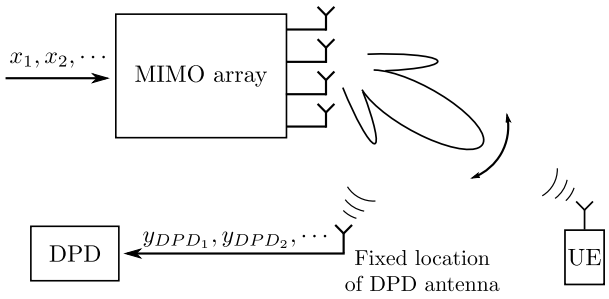

Fig. 1. Illustration of the proposed OTA-based data acquisition.

The rest of the article is organized as follows. In Section II, the proposed OTA-based indirect PA identification method is described. The construction of DPD is given in Section III. The simulation and experimental results are given in Sections IV and V, respectively, followed by a conclusion in Section VI.

II. Indirect Identification of MIMO PAs

In the existing DPD schemes of MIMO systems, couplers and attenuators are widely used to acquire the output of PAs in MIMO. Considering a large number of PAs in massive MIMO transmitters, it is unrealistic to deploy multiple couplers. To solve these issues, an OTA signal acquisition technique is proposed. As illustrated in Fig. 1, an external antenna, named DPD antenna, is set beside the transmitter antenna array to acquire the transmitted data from a fixed location. In real-time operation, the phase of the signals radiated from the antenna array changes according to the location of the user equipment (UE) and, thus, multiple blocks of data with different phase combinations of the PA outputs can be received by the DPD antenna. These data can then be used to reconstruct the signals from the PA outputs and to calibrate the DPD to linearize the signal at the user end. Compared with the existing methods, this proposed solution avoids the use of couplers or switches in the transmitter, thereby alleviates insertion loss and greatly decreases hardware implementation cost. Please note that the OTA data acquisition architecture itself shown in Fig. 1 is not new, and it has been presented in the literature, e.g., in [17]. However, how to utilize this architecture to reconstruct the PA outputs and calibrate DPD in real-time has not been presented before, which we will discuss in detail in the following.

A. Signal Model of MIMO Array

In massive MIMO systems, different array configurations, e.g., linear array or 2-D array, may be deployed. These arrays may have different radiation patterns, but they all share the same operation principle, namely, by adjusting amplitude and phase of the transmit signals radiated from multiple antennas

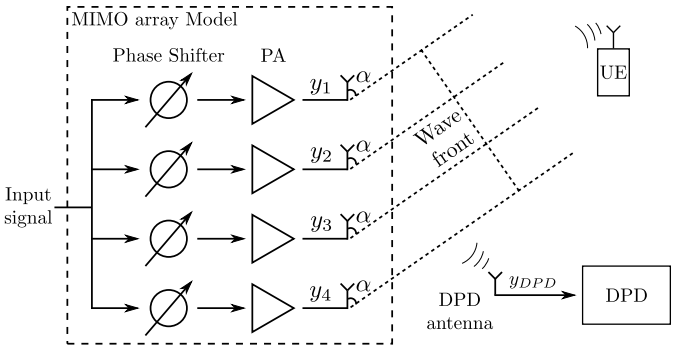

Fig. 2. Signal model of MIMO array.

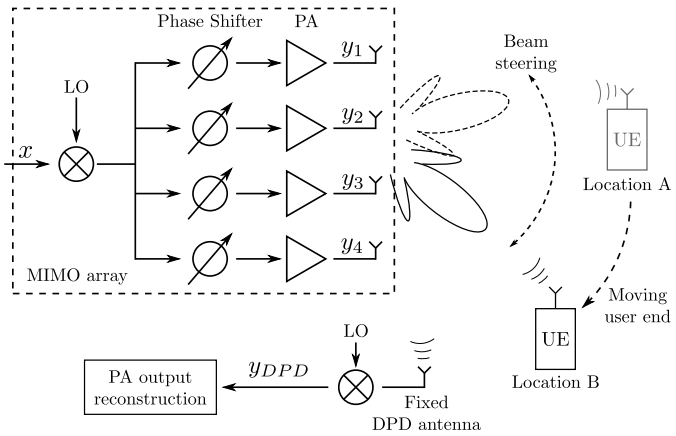

Fig. 3. Illustration of the UE movement.

to form beams pointing to user directions. Since the channel in the space is linear, the signals received at the user end can be considered as linear combinations of the antenna outputs [1]. For simplicity, we consider a uniform linear array (ULA), shown in Fig. 2, as an example in the following analysis. The derivation for other arrays can be conducted in the same way. The ULA consists of N antenna elements with equal spacing d, and each succeeding RF chain has a β progressive phase increase relative to the preceding one, i.e., the phase shifts in RF chains are $0, \beta, 2\beta, \ldots, (N-1)\beta$. The channel effects are considered as phase shifts only in the system model and all signals are expressed in complex baseband equivalent format. We also assume that all the RF chains use the same input data, which is a single-user case here. The multiuser case using multiple data streams can be extended later.

Assuming the input signal is x and the transfer function for the nth PA is H_n, the output of nth RF chain at the input of antenna can be expressed as

$$y_n = H_n[xe^{j(n-1)\beta}] = H_n[x]e^{j(n-1)\beta}. \tag{1}$$

The far-field transmitted signal in the direction angle α is

$$y_{\mathrm{RX}} = \sum_{n=1}^{N} H_n[x]e^{j(n-1)\beta}p_n(\alpha) \tag{2}$$

where $p_n(\alpha)$ represents phase shifts induced by the channel and can be calculated by

$$p_n(\alpha) = e^{j(n-1)\theta} = e^{j(n-1)kd\cos\alpha} \tag{3}$$

where θ is the progressive phase shift in the channel. The far-field transmitted signal is maximized when the phase shifts in phase shifter compensate for that caused in antenna array and channels, which means

$$e^{j(n-1)\beta}p_n(\alpha) = e^{j(n-1)\beta}e^{j(n-1)kd\cos\alpha} = 1. \tag{4}$$

Therefore, ideally, in the main beam direction, we have

$$y_{\mathrm{RX}} = \sum_{n=1}^{N} H_n[x]. \tag{5}$$

Correspondingly, when the signal is received from a different direction, e.g., in the angle of α_D, which can be assumed to be the direction of the DPD antenna, the received signal is

$$y_{\mathrm{DPD}} = \sum_{n=1}^{N} H_n[x]e^{j(n-1)\beta}p_n(\alpha_D) \tag{6}$$

or it can be expressed as

$$y_{\mathrm{DPD}} = \sum_{n=1}^{N} H_n[x]e^{j(n-1)\beta}e^{j(n-1)\theta_D} \tag{7}$$

where $\theta_D = kd\cos\alpha_D$.

B. PA Output Reconstruction

In real environment, the phase of transmitted signals changes based on the movement of the UE. For instance, if the UE moves from location A to location B, shown in Fig. 3, the progressive phase shift in the phase shifters will change from β_A to β_B to ensure that the main beam is pointed to the new location. The output of nth RF chain, thus, will change from

$$y_n = H_n[xe^{j(n-1)\beta_A}] = H_n[x]e^{j(n-1)\beta_A}$$

to

$$y_n = H_n[xe^{j(n-1)\beta_B}] = H_n[x]e^{j(n-1)\beta_B}.$$

Since the DPD antenna is located at the fixed location, it will receive different data blocks with different phase shifts during the operation time. When the UE is at location A, the signal received by the DPD antenna is

$$y_{\mathrm{DPD}_A} = \sum_{n=1}^{N} H_n[x]e^{j(n-1)\beta_A}e^{j(n-1)\theta_D} \tag{8}$$

while at location B, the signal is changed to

$$y_{\mathrm{DPD}_B} = \sum_{n=1}^{N} H_n[x]e^{j(n-1)\beta_B}e^{j(n-1)\theta_D}. \tag{9}$$

It is shown that y_{DPD} combines information of all PAs, and the combining weights change with the main beam direction. Because the phase shift in the phase shifters can be known, after multiple movements and measurements, it is possible to

use the signals received at the DPD antenna to reconstruct the output of each PA in the input of antenna.

Let us assume that the transmitter steers to a different main beam direction M times and M measurements are performed at the DPD antenna. β_m is the progressive phase increase between two adjacent antenna elements in the mth measurement. For input data $\mathbf{x}$, the received data blocks at DPD antenna can be represented by

$$\mathbf{Y_{DPD}} = \mathbf{H}[\mathbf{x}]\Psi_{\boldsymbol{\beta}} \tag{10}$$

where

$$\mathbf{Y_{DPD}} = \begin{bmatrix} \mathbf{y_{DPD_1}} & \mathbf{y_{DPD_2}} & \cdots & \mathbf{y_{DPD_M}} \end{bmatrix}$$

$$\boldsymbol{\Psi_\beta} = \begin{bmatrix} 1 & 1 & \cdots & 1 \\ e^{j(\beta_1+\theta_D)} & e^{j(\beta_2+\theta_D)} & \cdots & e^{j(\beta_M+\theta_D)} \\ e^{j2(\beta_1+\theta_D)} & e^{j2(\beta_2+\theta_D)} & \cdots & e^{j2(\beta_M+\theta_D)} \\ \vdots & & & \\ e^{j(N-1)(\beta_1+\theta_D)} & e^{j(N-1)(\beta_2+\theta_D)} & \cdots & e^{j(N-1)(\beta_M+\theta_D)} \end{bmatrix}$$

$$\mathbf{H}[\mathbf{x}] = \begin{bmatrix} H_1[\mathbf{x}] & H_2[\mathbf{x}] & \cdots & H_N[\mathbf{x}] \end{bmatrix}.$$

In (10), $\mathbf{Y_{DPD}}$ and $\boldsymbol{\Psi_\beta}$ are known, and the output of PA, $\mathbf{H}[\mathbf{x}]$, can be calculated by using least squares (LS)

$$\mathbf{H}[\mathbf{x}] = \left(\boldsymbol{\Psi_\beta}^H \boldsymbol{\Psi_\beta}\right)^{-1} \boldsymbol{\Psi_\beta}^H \mathbf{Y_{DPD}}. \tag{11}$$

C. Real-Time Operation With Forward Modeling

The proposed linear inversion in (11) can reconstruct the PA output, but it cannot be directly applied in real-time operation because it assumes that the same input data are transmitted repeatedly. To resolve this issue, in this article, we propose to extract the behavior of PAs with forward modeling. It is generally safe to assume that the PA characteristics do not change suddenly. In other words, within a reasonably short time period, e.g., seconds or minutes, the PA behavior is relatively stable and the PA model coefficients do not change with the input data or the main beam direction. In this case, we can represent the PA behavior using forward models in the data process, and we can then reconstruct the PA outputs and characterize the DPD in real time even if the input data streams are varying.

Let the mth input data be $\mathbf{x_m}$. The received signal at DPD antenna is

$$\mathbf{y_{DPD_m}} = \sum_{n=1}^{N} H_n[\mathbf{x_m}] e^{j(n-1)\beta_m} e^{j(n-1)\theta_D}. \tag{12}$$

Assume that the nonlinear behavior of each PA can be modeled by a PA behavioral model, the output of PA can be represented by $H_n[\mathbf{x_m}] = \mathbf{X_m c_n}$, where $\mathbf{X_m}$ includes all basis functions built by input signal $\mathbf{x_m}$ and $\mathbf{c_n}$ is the coefficients of nth PA. The received signal can be expressed as

$$\mathbf{y_{DPD_m}} = \sum_{n=1}^{N} \mathbf{X_m c_n} e^{j(n-1)\beta_m} e^{j(n-1)\theta_D}. \tag{13}$$

If we can observe M input data with different β, (13) can be written into matrix format

$$\mathbf{y_{DPD}} = \mathbf{X_\beta c_{PA}} \tag{14}$$

where

$$\mathbf{X_\beta} = \begin{bmatrix} \mathbf{X_1} & \mathbf{X_1} e^{j(\beta_1+\theta_D)} & \mathbf{X_1} e^{j2(\beta_1+\theta_D)} & \cdots & \mathbf{X_1} e^{j(N-1)(\beta_1+\theta_D)} \\ \mathbf{X_2} & \mathbf{X_2} e^{j(\beta_2+\theta_D)} & \mathbf{X_2} e^{j2(\beta_2+\theta_D)} & \cdots & \mathbf{X_2} e^{j(N-1)(\beta_2+\theta_D)} \\ \vdots & & & & \\ \mathbf{X_m} & \mathbf{X_m} e^{j(\beta_m+\theta_D)} & \mathbf{X_m} e^{j2(\beta_m+\theta_D)} & \cdots & \mathbf{X_m} e^{j(N-1)(\beta_m+\theta_D)} \end{bmatrix}$$

$$\mathbf{c_{PA}} = \begin{bmatrix} \mathbf{c_1} \\ \mathbf{c_2} \\ \vdots \\ \mathbf{c_N} \end{bmatrix}.$$

Equation (14) can be solved by using LS, and thus, the PA coefficients can be calculated as

$$\mathbf{c_{PA}} = \left(\mathbf{X_\beta}^H \mathbf{X_\beta}\right)^{-1} \mathbf{X_\beta}^H \mathbf{y_{DPD}}. \tag{15}$$

Once $\mathbf{c_{PA}}$ is known, the output of each PA can be reconstructed.

D. Complexity-Reduced Model Identification

Solving the inverse equation is straightforward, but large matrix operations can be costly. An improved algorithm is developed to reduce the computational complexity.

We can rewrite (13) as

$$\mathbf{y_{DPD_m}} = \mathbf{X_m} \sum_{n=1}^{N} \mathbf{c_n} e^{j(n-1)\beta_m} e^{j(n-1)\theta_D}. \tag{16}$$

If we make the following definition

$$\mathbf{c_{\beta_m}} \triangleq \sum_{n=1}^{N} \mathbf{c_n} e^{j(n-1)\beta_m} e^{j(n-1)\theta_D} \tag{17}$$

we can solve $\mathbf{c_{\beta m}}$ by

$$\mathbf{c_{\beta_m}} = \left(\mathbf{X_m}^H \mathbf{X_m}\right)^{-1} \mathbf{X_m}^H \mathbf{y_{DPD_m}}. \tag{18}$$

If we gather M data blocks, (17) can be written in matrix format

$$\mathbf{c_\beta} = \mathbf{c'_{PA}} \boldsymbol{\Psi_\beta} \tag{19}$$

where

$$\mathbf{c_\beta} = \begin{bmatrix} \mathbf{c_{\beta_1}} & \mathbf{c_{\beta_2}} & \cdots & \mathbf{c_{\beta_M}} \end{bmatrix}$$
$$\mathbf{c'_{PA}} = \begin{bmatrix} \mathbf{c_1} & \mathbf{c_2} & \cdots & \mathbf{c_N} \end{bmatrix}.$$

The PA coefficients can be calculated as

$$\mathbf{c'_{PA}} = \mathbf{c_\beta} \boldsymbol{\Psi_\beta}^H \left(\boldsymbol{\Psi_\beta} \boldsymbol{\Psi_\beta}^H\right)^{-1}. \tag{20}$$

A large-scale LS problem is transformed into a few smaller ones, so the total complexity compared to the previous algorithm is reduced approximately by a factor of N^2.

E. Mutual Coupling Consideration

One practical problem caused by massive MIMO systems is mutual coupling between elements in the antenna array. In this part, we prove that the proposed MIMO DPD scheme can achieve robust reconstruction performance under the mutual coupling effect.

In transmitters with low isolation, the effects of mutual coupling on transmitted signals change with the beam-steering angle. Assume that the mutual coupling coefficients are

$$\mathbf{H} = \begin{bmatrix} h_{11} & h_{12} & \cdots & h_{1N} \\ h_{21} & h_{22} & \cdots & h_{2N} \\ \vdots & & & \\ h_{N1} & h_{N2} & \cdots & h_{NN} \end{bmatrix}$$

(13) can be rewritten with mutual coupling as

$$\mathbf{y'_{DPD_m}} = \sum_{n=1}^{N}\sum_{k=1}^{N} h_{nk}\, y_{PA_k} e^{j(k-1)\beta_m} p_n(\alpha_D). \tag{21}$$

Accordingly, (17) can be rewritten as

$$\mathbf{c'_{\beta_m}} = \sum_{n=1}^{N}\sum_{k=1}^{N} h_{nk}\mathbf{c_k} e^{j(k-1)\beta_m} p_n(\alpha_D). \tag{22}$$

Write (22) into matrix format

$$\mathbf{c'_{\beta_m}} = \begin{bmatrix} \mathbf{c_1} & \mathbf{c_2} & \cdots & \mathbf{c_N} \end{bmatrix} \mathbf{h_{mc}^{(m)}} \tag{23}$$

where

$$\mathbf{h_{mc}^{(m)}} = \left[\sum_{n=1}^{N} h_{n1} e^{j(n-1)\theta}, \ldots, \sum_{n=1}^{N} h_{nk} e^{j[(k-1)\beta_m + (n-1)\theta]}, \ldots \right]^T.$$

Gathering $\mathbf{h_{mc}^{(m)}}$ calculated from all data blocks, we could stack the vectors to build matrix $\mathbf{H_{mc}}$ column by column. Equation (19) can be rewritten as

$$\mathbf{c'_\beta} = \mathbf{c'_{PA}} \mathbf{H_{mc}}. \tag{24}$$

If we still follow the procedures in (20) to estimate the forward model coefficients, the estimated coefficients are

$$\begin{aligned} \mathbf{c_{PA_{mc}}} &= \mathbf{c'_\beta} \left(\mathbf{\Psi_\beta}^H \mathbf{\Psi_\beta} \right)^{-1} \mathbf{\Psi_\beta}^H \\ &= \mathbf{c'_{PA}} \mathbf{H_{mc}} \mathbf{\Psi_\beta}^H \left(\mathbf{\Psi_\beta} \mathbf{\Psi_\beta}^H \right)^{-1}. \end{aligned} \tag{25}$$

We define the deviation from the ideal coefficients as

$$\Delta \triangleq \mathbf{H_{mc}} \mathbf{\Psi_\beta}^H \left(\mathbf{\Psi_\beta} \mathbf{\Psi_\beta}^H \right)^{-1}.$$

It reveals that $\mathbf{\Delta}$ is the LS solution to the problem

$$\mathbf{\Delta} \mathbf{\Psi_\beta} = \mathbf{H_{mc}}. \tag{26}$$

As is proven in the Appendix

$$\mathbb{E}\,\mathbf{\Delta} = \begin{bmatrix} \sum_{n=1}^{N} h_{n1} e^{j(n-1)\theta} & 0 & \cdots \\ 0 & \sum_{n=1}^{N} h_{n2} e^{j(n-2)\theta} & \cdots \\ \vdots & \vdots & \ddots \end{bmatrix}. \tag{27}$$

All off-diagonal elements are zero, and the diagonal elements only depend on the coupling coefficients and the direction of DPD receiver, which are both constant after the deployment.

Therefore, compared with $\mathbf{c_{PA}}$, each element of $\mathbf{c_{PA_{mc}}}$ is simply scaled by a scalar. As the scaling factor is constant, it can be easily compensated in the calibration process. Therefore, our proposed algorithm can work robustly even under the situations where the coupling matrix is unknown to the system.

F. Other Practical Considerations

1) DPD Observation Receiver: The deployment of the proposed method requires a proper choice of the location of DPD observation receiver. Though the theoretical derivation assumes the receiver locates in the far field of the antenna array, this requirement can be greatly relaxed in practice. According to [22], the linear superposition rule for calculating antenna pattern is valid as long as the receiving antenna is in the far-field of the antenna element. Thus, the derivation is still valid if DPD antenna is in far field of antenna element but near field of the whole antenna array. These observations suggest that the DPD antenna can be placed very close to the mmWave TX array, greatly reducing the integration cost of the proposed DPD architecture.

Another issue for DPD observation receiver design concerns the beam-steering problem. In 5G massive MIMO transmitters, the direction of transmitted signals is changed with the location of users, and the radiation pattern of TX array will change accordingly. As a result, the received signal power at the DPD receiver varies with main beam directions. Therefore, a large dynamic range is required for the receiver. However, because the DPD antenna is fixed in a known location, preselection and calibration can be conducted to choose suitable angles to receive the signal. To further relax the dynamic range requirement, variable gain amplifier (VGA) for power normalization can be used at the early stage of the DPD receiver. A lookup table (LUT) can be built to record the antenna radiation pattern and the corresponding complex-valued array gain in the direction of DPD antenna. With the assistance of LUT, the array gain will be normalized by the VGA and subsequently restored in the digital domain.

2) Effect of MIMO Channels: The time variation and noise in channels affect the amplitudes and phase of received signals at UEs, as well as that at DPD antenna. However, the proposed DPD method can work well in such noisy communication systems. On one hand, the channel between the transmitter and DPD observation receiver is fixed, so the potential performance degradation can be greatly alleviated by calibration. On the other hand, even in systems with the high noise level, the proposed DPD method can suppress the influence by building forward models with signals from more directions.

In massive MIMO transmitters, the beam update speed is expected to be fast. It may pose severe problems to the existing DPD methods based on the time-division acquisition of PA output. However, in the proposed scheme, the rapid beam changing actually helps collect signals from more directions, which decreases the impact of channel noise and increases the

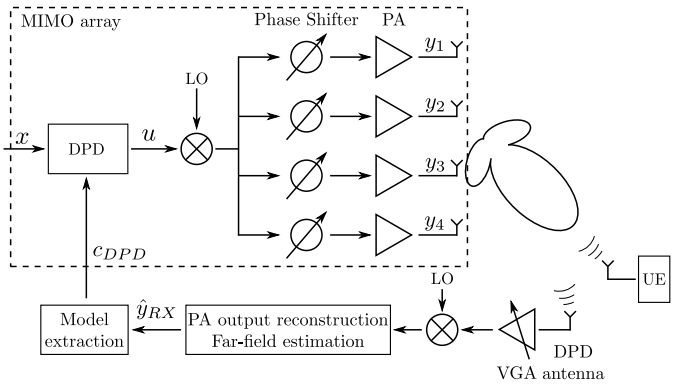

Fig. 4. Architecture of the proposed MIMO DPD system.

accuracy of reconstructed signals, and thereby realize better linearization of far-field signals.

III. DPD Construction

In a DPD system, data reconstruction targets can be chosen according to the aim of linearization. In recent works, the main beam and PA outputs are two common linearization targets. In this section, the application of the proposed MIMO DPD method with different linearization targets will be explained.

A. DPD for Beam-Oriented Linearization

The beam-oriented linearization approach [13] treats all the PAs in the array as a single input and a single combined output system. It uses the far-field user-end signal as the target, and thus, only the signal at the main beam direction is linearized. The proposed MIMO DPD method consists of two main elements, far-field estimation and DPD coefficient extraction, as shown in Fig. 4. The output of each PA can be estimated with the input signal and the forward models extracted as discussed in Section II. Far-field received signals in any direction can be estimated based on the output of each PA and channel information. DPD coefficients are identified with the estimated far-field received signals.

1) Far-Field Distortion Prediction: The nonlinear behavior of PAs has been modeled by behavioral models. Considering channel effect, far-field main beam signal is the linear combination of transmitted signals at antennas. The regression matrix $\mathbf{U}$ can be built using PA input signal $\mathbf{u}$ and the forward models extracted in Section II. The estimated main beam signal is

$$\hat{\mathbf{y}}_{\mathrm{RX}} = \mathbf{U}\sum_{n=1}^{N}\mathbf{c_n}. \tag{28}$$

Apart from the prediction of far-field main beam distortion, signals received at other direction can also be predicted. In the α direction, the estimated far-field received signals are

$$\hat{\mathbf{y}}_{\mathrm{RX}} = \mathbf{U}\sum_{n=1}^{N}\mathbf{c_n}e^{j(n-1)\beta}p_n(\alpha). \tag{29}$$

2) Linearization of Far-Field Received Signal: To linearize the main beam, the estimated received signal $\hat{y}_{\mathrm{RX}}$ is used as the linearization reference. It is also possible to set an artificial target by adding up signals from more than one directions in order to achieve balanced linearization performance across multiple directions.

The remaining procedures of linearization are the same as the conventional DPD architectures. The proposed method works with any existing DPD models, and both direct learning and indirect learning algorithms can be used to extract the model coefficients. For example, in indirect learning, the regression matrix of postinverse model, $\mathbf{Y}$, can be built by feeding $\hat{\mathbf{y}_{\mathrm{RX}}}$ to the DPD model, and the DPD coefficients can be solved by

$$\mathbf{c_{DPD}} = (\mathbf{Y}^H\mathbf{Y})^{-1}\mathbf{Y}^H\mathbf{u} \tag{30}$$

where u is the output of DPD, and in the next iteration, the DPD output can be updated as

$$\mathbf{u} = \mathbf{X}\mathbf{c_{DPD}}. \tag{31}$$

B. DPD for Full-Angle Linearization

In a MIMO system, each PA typically has different nonlinear characteristics. Therefore, it is not possible to linearize all PAs with only one DPD. The beam-oriented DPD linearizes far-field main beam signals with low hardware cost, but it is unable to remove distortions in other spatial directions. For better distortion cancellation capabilities, full-angle linearization scheme [21] can be employed to fulfill the stringent linearity requirement across all spatial directions in 5G mmWave MIMO transmitters.

To ensure linear response in all directions, all PAs in the array must be linearized simultaneously. Traditionally, full-angle linearization is achieved by linearizing each PA separately. Reference [21] proposed a novel two-step DPD scheme that has much lower complexity and enables the potential application to hybrid beamforming systems.

The method works as follows. In the first step, all but the first PAs are tuned by a tuning box to remove the nonlinear behavior variations between different PAs. After forcing all PAs to have the same characteristics, a common DPD is employed to simultaneously linearize all PAs. The tuning boxes can be implemented in either analog or digital domain, making the approach also applicable to hybrid beamforming.

1) PA Reconstruction: Unlike beam-oriented DPD, full-angle linearization scheme produces separate predistorted signals for each PA. In the proposed improved reconstruction algorithm, however, the PAs are assumed to share the same input signal. To solve this conflict, we propose to build the forward models using the original input signal, instead of the actual input signal of PA. Thus, the output of PA is always modeled by $\mathbf{Xc_n}$, where matrix $\mathbf{X}$ is built by input signal $\mathbf{x}$, rather than predistorted signal $\mathbf{u}$. In this way, the forward model actually characterizes the cascade system of both DPD and PA, and the estimated PA outputs are still accurate. It is worth noting that all procedures in Section II are still valid,

and the only difference is that the input signals used to build forward models are changed.

2) Linearization of Each PA: To update DPD coefficients, all PAs' outputs are required. Based on the reconstruction algorithm, the estimated PA output in the nth RF chain is

$$H_n[\mathbf{u}] = \mathbf{X}\mathbf{c_n}. \tag{32}$$

The common DPD block can be extracted using the standard DPD parameter estimation methods, e.g., LS. Similarly, the tuning box can be extracted by

$$\mathbf{c_{DPD_n}} = \left(\mathbf{Y_n}^H\mathbf{Y_n}\right)^{-1}\mathbf{Y_n}^H\mathbf{u_n} \tag{33}$$

where $\mathbf{u_n}$ is the output of nth tuning box, and $\mathbf{Y_n}$ is built by first feeding $H_n[\mathbf{u}]$ to the common DPD model and then generating the required basis functions. Applying the DPD coefficients, the predistorted signal can be updated as

$$\mathbf{u_n} = \mathbf{X}\mathbf{c_{DPD_n}}. \tag{34}$$

IV. Simulation Results

The performance of the proposed MIMO DPD scheme will be analyzed with beam-oriented linearization and full-angle linearization based on 1×8 ULA (a subarray with eight RF chains) and 1×32 ULA (a subarray with 32 RF chains) with element spacing $\lambda/2$ at 28 GHz. To model PAs, memory polynomials (MP) models [23] with different nonlinear characteristics were used. For DPD, magnitude-selective affine (MSA) model [24] with $M = 1$ and $K = 6$ was considered. Input waveforms were 20-MHz long-term evolution (LTE) input signals with peak-to-average power ratio (PAPR) of 6.5 dB.

In MATLAB simulation, the main beam was steered to different directions by adjusting the phase shifts of each simulated RF chain. The DPD antenna was fixed at 120° direction. After capturing a number of data blocks, the forward modeling and DPD model extraction were performed. Afterward, the extracted DPD coefficients were applied to the input signal for the next iteration. To simulate the linearization performance, the estimated and actual PA outputs were compared. Similar comparisons were also made on the far-field signals.

A. Performance of Proposed Method in Beam-Oriented DPD

1) 1×8 ULA: To simulate the proposed method, the main beam was steered to 35°, 45°, 55°, 65°, 75°, 85°, 95°, and 105° to produce signals for reconstruction. Fig. 5(a) shows the direction of DPD antenna relative to the main beam in each measurement. Fig. 5(c) and (d) draws a comparison between reconstructed and actual outputs of the first and the fourth PAs, respectively. The corresponding NMSE values are summarized in Table I, showing that the reconstructed PA outputs have very good agreement with actual PA outputs. To this step, the proposed DPD method has obtained the same PA output information as the traditional DPD methods where couplers are used. Based on the forward models, far-field signal at any direction can be estimated. Taking the main beam signal as an example, Fig. 5(b) shows that the estimated far-field main beam signals agree with the actual main beam

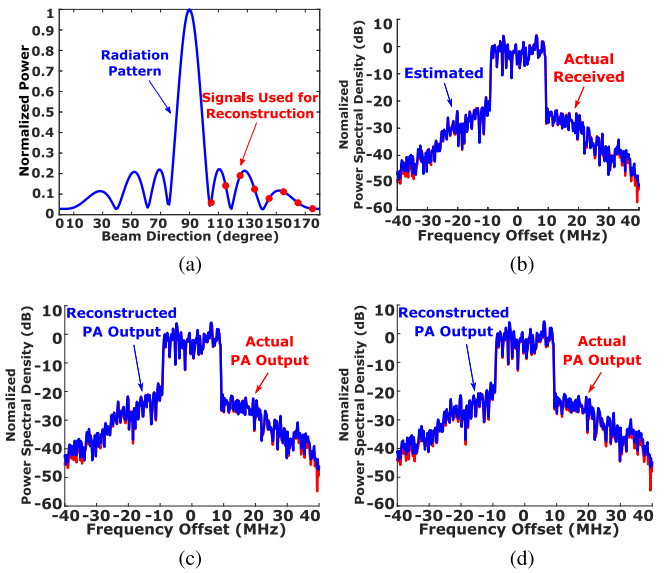

Fig. 5. Simulation results of signal reconstruction with beam-oriented DPD in 1×8 ULA. (a) Radiation pattern and signals used for reconstruction. (b) Reconstruction of far-field main beam signals. (c) Reconstruction of output of the first PA. (d) Reconstruction of output of the fourth PA.

TABLE I
Simulation Results of the Proposed Reconstruction Method

	NMSE (dB) @ PA Output			NMSE (dB) @ Main Beam
	min	max	mean	
1×8 ULA	-38.12	-35.82	-36.78	-37.60
1×32 ULA	-38.71	-34.97	-36.50	-36.60

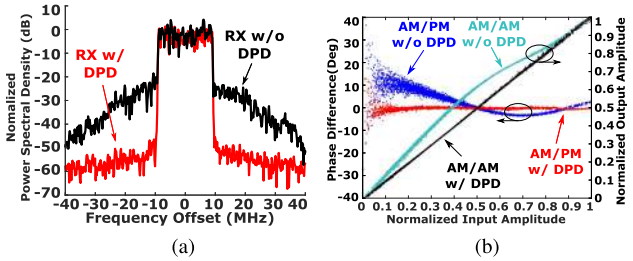

Fig. 6. Simulated linearization performance of far-field main beam signals with beam-oriented DPD in 1×8 ULA. (a) Spectrum comparison. (b) AM–AM and AM–PM results.

signals, and NMSE between them is −37.60 dB. Fig. 6(a) presents the linearity of the main beam signal without and with the proposed DPD method. The proposed DPD method improves the linearity in the desired direction and achieves −52.15/−49.48 dBc ACPR. The detailed linearization performance is summarized in Table II.

2) 1×32 ULA: For 1×32 ULA, MATLAB simulation results also show very good performance in the reconstruction of PA outputs and far-field main beam signals, as well as the linearization of main beam signals.

Main beam directions used for reconstruction were uniformly distributed within the range from 35° to 160°. Fig. 7(c) and (d) compares the reconstructed and the actual outputs of the two PAs in the array. NMSE values between

TABLE II

SIMULATED LINEARIZATION PERFORMANCE OF THE PROPOSED METHOD WITH BEAM-ORIENTED DPD

	NMSE (dB) @ Main Beam	ACPR (dBc) @ Main Beam
1×8 ULA w/o DPD	-13.84	-27.85/-28.05
1×8 ULA w/ DPD	-42.39	-52.15/-49.48
1×32 ULA w/o DPD	-13.39	-27.31/-27.57
1×32 ULA w/ DPD	-41.42	-50.96/-49.09

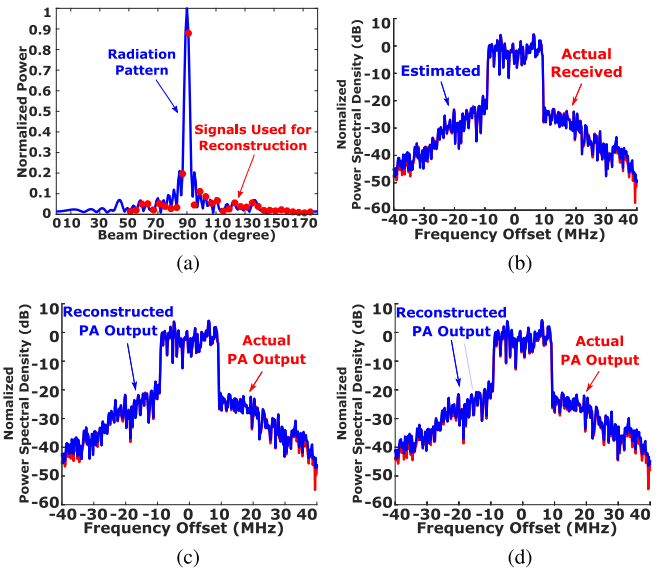

Fig. 7. Simulation results of signal reconstruction with beam-oriented DPD in 1×32 ULA. (a) Radiation pattern and signals used for reconstruction. (b) Reconstruction of far-field main beam signals. (c) Reconstruction of output of the first PA. (d) Reconstruction of output of the fourth PA.

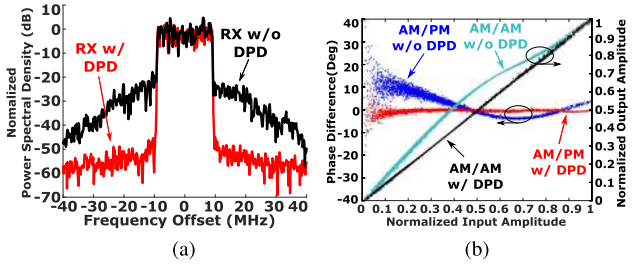

Fig. 8. Simulated linearization performance of far-field main beam signals with beam-oriented DPD in 1×32 ULA. (a) Spectrum comparison. (b) AM–AM and AM–PM results.

them are listed in Table I. Fig. 7(b) shows that the estimated main beam signals agree with the actual main beam signals and NMSE between them reaches -36.60 dBc. Fig. 8(a) presents the linearity of the main beam signal without and with the proposed DPD method. The proposed DPD method improves the linearity in the desired direction and achieves $-50.96/-49.09$ dBc ACPR. More details are listed in Table II.

B. Performance of Proposed Method in Full-Angle DPD

A 1×8 ULA was simulated to verify the proposed method in full-angle DPD. Radiation pattern and signals

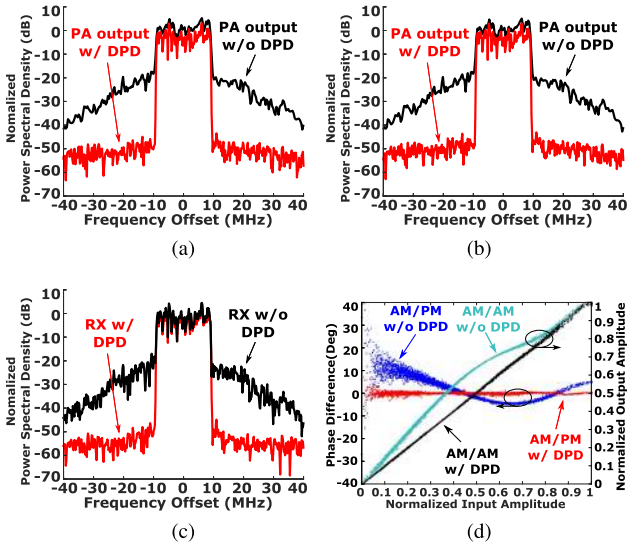

Fig. 9. Simulated linearization performance with full-angle DPD in 1×8 ULA. (a) Spectrum comparison of the first PA. (b) Spectrum comparison of the fourth PA. (c) Spectrum comparison of far-field main beam signals. (d) AM–AM and AM–PM results of far-field main beam signals.

TABLE III

SIMULATED LINEARIZATION PERFORMANCE OF THE PROPOSED METHOD WITH FULL-ANGLE DPD IN 1×8 ULA

	NMSE (dB)			ACPR (dBc)		
	min	max	mean	min	max	mean
w/o DPD	-15.39	-12.42	-13.76	-27.00	-24.73	-25.81
w/ DPD	-39.67	-37.11	-37.66	-55.38	-47.15	-51.38

used for reconstruction were the same as that in simulation for the beam-oriented DPD method shown in Fig. 5(a). PA reconstruction procedures in full-angle DPD were also the same as that in beam-oriented DPD. Fig. 9(a) and (b) show good linearity of PA output with the proposed full-angle DPD method. Performance of the main beam signal is confirmed in Fig. 9(c) and (d). The achieved NMSE and ACPR values are presented in Table III.

C. Effect of Mutual Coupling

Effect of mutual coupling between antenna elements was considered in the MATLAB simulation. In the simulation, the coupling effect was set as a constant but unknown factor. A matrix identifying mutual coupling coefficients was multiplied with the PA output signals before transmitted to UE. In the simulation, only the coupling from one adjacent antenna element from each side was considered, and the coupling coefficient was set as 0.5, which means that half of the signals from the adjacent RF chain is coupled.

As listed in Table IV, even with such high coupling factors, the mutual coupling has little influence on the reconstructed PA outputs and far-field main beam signals, compared with the results of ULA 1×32 in Table I.

TABLE IV
SIMULATED RECONSTRUCTION RESULTS OF THE PROPOSED METHOD WITH COUPLING AND CHANNEL NOISE IN 1 × 32 ULA

	NMSE (dB) @ PA Output			NMSE (dB) @ Main Beam
	min	max	mean	
w/ coupling	-44.52	-36.02	-39.50	-37.37
w/ noise	-45.04	-35.73	-38.58	-39.14

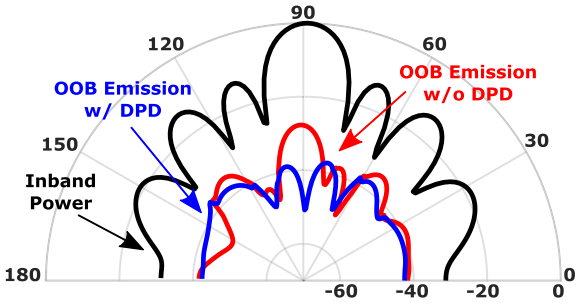

Fig. 10. In-band power, OOB emission pattern without and with beam-oriented DPD in 1 × 8 ULA for all spatial directions.

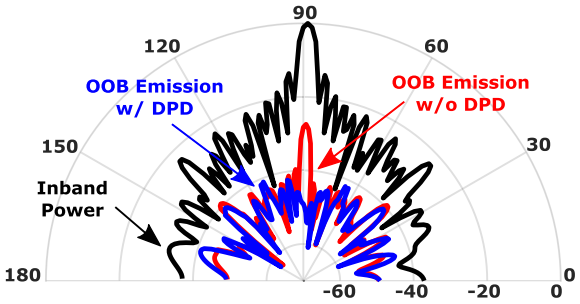

Fig. 11. In-band power, OOB emission pattern without and with beam-oriented DPD in 1 × 32 ULA for all spatial directions.

D. Effect of MIMO Channel Noise

The effect of massive MIMO channel condition on the proposed DPD method was analyzed based on the array with 1 × 32 ULA. To model the influence of noise in massive MIMO channel, a random variation was added to the phase and amplitude of received signals at user end and DPD antenna, and the SNR was set as −60 dB. The simulation results in Table IV show that the noise does not affect the performance of the proposed method.

E. Effect of Proposed DPD on Other Directions

In this part, we analyze how the in-band power and out-of-band (OOB) emissions in all different spatial directions behave after applying the proposed DPD. Figs. 10–12 show that the OOB emissions of massive MIMO transmitters generally follow the beam pattern of the array before DPD. OOB emissions are more powerful in the direction of the intended receiver but weaker in other directions.

1) In Beam-Oriented DPD: After applying the beam-oriented DPD method, the OOB emissions are attenuated significantly in the main beam direction as they are set as the linearization targets, as shown in Figs. 10 and 11. Besides, the simulation results also show that the beam-oriented DPD scheme does not fully remove distortions in other directions.

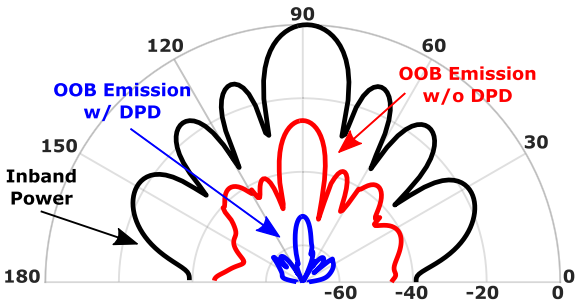

Fig. 12. In-band power, OOB emission pattern without and with full-angle DPD in 1 × 8 ULA for all spatial directions.

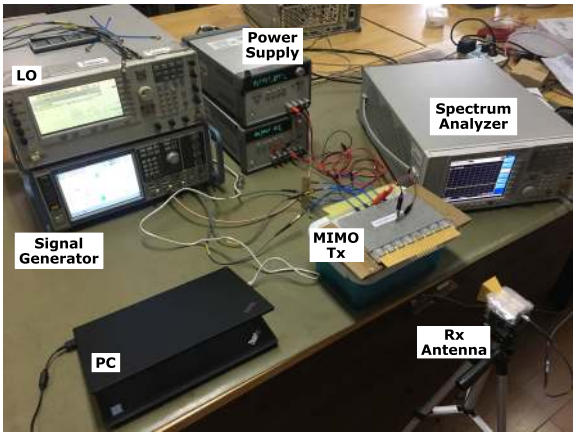

Fig. 13. Proposed MIMO DPD test bench.

2) In Full-Angle DPD: Fig. 12 shows that the OOB emissions are attenuated in all spatial directions after applying the full-angle DPD method. Compared with beam-oriented DPD, full-angle DPD achieves better overall linearization performance.

V. EXPERIMENTAL RESULTS

To verify the proposed idea, several experiments have been carried out, and the results are presented in this section.

A. Experimental Setup

Due to limited hardware resource available, we only conducted tests on 1×2 ULA and 1×4 ULA cases. The test bench was set up as shown in Fig. 13. For setup of a 1×2 ULA, two baseband input signals with bandwidth of 20 MHz and PAPR of 5.5 dB were generated by the software MATLAB in PC and downloaded to the two signal channels provided by a dual-channel signal generator (R&S SMW200A). The two channels can be phase-shifted separately to realize the beamforming operation. In 1×4 ULA test, because of instrument limitations, all RF chains share one baseband channel, i.e., the baseband signal generated by the signal generator was split into four ways by a one-to-four power divider. The same test signal as 1 × 2 ULA tests was used.

In both cases, the baseband signals were upconverted to IF @ 5.5 GHz and fed into the designed RF front end. In this module, all signals were again upconverted to 27 GHz by 10.75-GHz local oscillator (LO) signals generated by a signal generator (Keysight E8267D) with a power divider and fed into

corresponding PAs with the average output power of around 14 dBm. PAs not in use were turned off to avoid crosstalk. Next, the Tx chain outputs were fed into the antenna elements to form the desired radiation pattern. In the receiver side, one horn antenna was employed for OTA test and a spectrum analyzer (Keysight N9030A) was utilized to capture the OTA outputs. Both the outputs and the inputs were sent back to the PC for DPD procedures.

B. System Calibration

Hardware impairments that exist in all physical implementations of wireless systems and especially in massive MIMO systems may, in practice, lead to severe performance losses [25]. Therefore, calibration procedures were employed.

The calibration process consisted of two stages, namely, delay calibration and phase calibration. The first stage was intended to cancel the delay mismatch between different channels of the signal generator, while the second stage aimed to align the phase between different RF chains.

In the delay calibration stage, uncorrelated signals were sent to the transmitter. The received OTA signals were time-aligned with the input signals one by one to determine the delay of each baseband channel. After obtaining the delay values, the time delay mismatch can be compensated by delaying the transmitted signals in MATLAB before sending them to the instrument.

In the phase calibration stage, the same data were fed to the RF chains. After obtaining the OTA signal, the output of each PA was individually captured over the air. As time delay has already been calibrated in the previous stage, signals received at OTA antenna and output of each PA can be used to calculate gain and phase difference across different RF chains by LS. Accordingly, gain and phase differences across RF chains can be compensated by either inversely scaling the corresponding transmitted baseband signals or preprocessing the received OTA data before reconstruction algorithm.

C. Measurement Results

In the experimental tests of 1×2 ULA, the main beam was steered to different directions by adjusting the phase shifts of the input signal chains. The DPD antenna was fixed at a specific location while receiving signals of different main beam directions. After capturing a number of data blocks, the forward modeling and DPD model extraction were performed. To verify linearization performance, the main beam direction was set to point to the DPD antenna so that the main beam signal can be acquired and evaluated without moving the DPD antenna.

For 1×4 ULA, however, due to the lack of mmWave phase shifters, the main beam was fixed at 90°, and beam steering was not available. As all RF chains shared one baseband channel, only beam-oriented DPD was evaluated. To validate the proposed reconstruction algorithm, the location of the receiver was moved to different locations to capture data with different phase information. The receiver was finally moved back to 90° to verify the performance in the main beam direction.

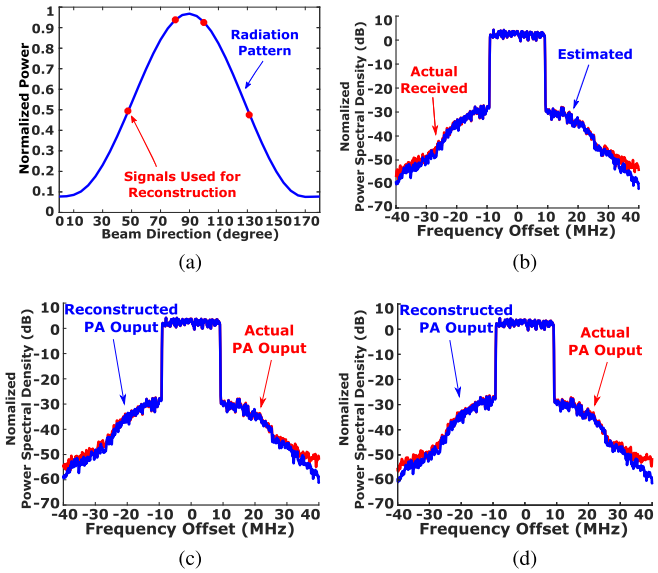

Fig. 14. Measurement results of signal reconstruction in 1×2 ULA. (a) Radiation pattern and signals used for reconstruction. (b) Reconstruction of far-field main beam signals. (c) Reconstruction of output of the first PA. (d) Reconstruction of output of the second PA.

TABLE V
MEASUREMENT RESULTS OF THE PROPOSED RECONSTRUCTION METHOD

	NMSE (dB) @ PA Output	NMSE (dB) @ Main Beam
1×2 ULA	-36.93 / -40.04	-40.54
1×4 ULA	-34.37 / -35.77 / -39.41 / -38.76	-41.36

In both cases, the PA output was reconstructed using the proposed algorithm. Based on the estimated PA output, far-field signals at specified direction can be estimated with channel information, as summarized in Table V. Then, they were used to extract DPD coefficients. Afterwards, the extracted coefficients were applied to the input signal for the next iteration.

Individual PA outputs were also captured. Baseband signals were sent by single RF chain separately, and the RF chains were switched on one at a time. Time delay, phase shifts, and power loss due to channel effect can be removed by synchronization and normalization. Note that the captured individual PA outputs were only used for comparison purpose, and they were not used in reconstruction or DPD.

1) Beam-Oriented DPD for 1×2 ULA: To build forward models, the main beam is steered to 50°, 80°, 100°, and 130°. The spectral results are demonstrated in Fig. 14(c) and (d), showing good agreement between the reconstructed and actual outputs of each PA. The NMSE of them were -36.93 and -40.04 dB, respectively. As shown in Fig. 14(b), estimated far-field main beam signal also agrees with actual far-field signals with NMSE reaching -40.54 dB.

The performance of the proposed DPD method is illustrated in Fig. 15. It is shown that the proposed MIMO DPD method achieves an ACPR of $-51.27/-50.09$ dBc. Detailed performance metrics are listed in Table VI.

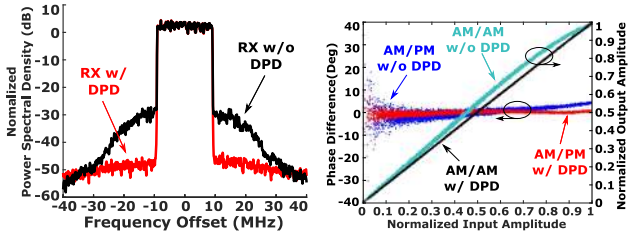

(a) (b)

Fig. 15. Measured linearization performance of far-field main beam signals with beam-oriented DPD in 1 × 2 ULA. (a) Spectrum comparison. (b) AM–AM and AM–PM results.

TABLE VI

MEASURED PERFORMANCE OF THE PROPOSED METHOD WITH BEAM-ORIENTED DPD

	NMSE (dB) @ Main Beam	ACPR (dBc) @ Main Beam
1 × 2 ULA w/o DPD	-26.31	-37.11/-36.39
1 × 2 ULA w/ DPD	-40.67	-51.27/-50.09
1 × 4 ULA w/o DPD	-24.95	-35.15/-35.11
1 × 4 ULA w/ DPD	-38.57	-49.98/-47.88

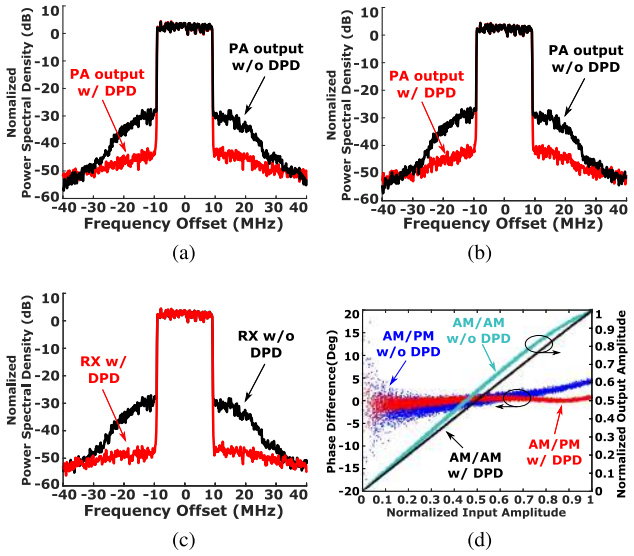

(a) (b)

(c) (d)

Fig. 16. Measured linearization performance with full-angle DPD in 1×2 ULA. (a) Spectrum comparison of the first PA. (b) Spectrum comparison of the second PA. (c) Spectrum comparison of far-field main beam signals. (d) AM–AM and AM–PM results of far-field main beam signals.

2) Full-Angle DPD for 1 × 2 ULA: OTA data with the same main beam directions as previous tests were collected. The PA linearization results of the full-angle DPD method are illustrated in Fig. 16(a) and (b) and Table VII. It is shown that DPD successfully linearized both PAs in the array and achieves an ACPR of −49.30/−47.77 and −47.93/−46.83 dBc, respectively. The far-field main beam signal is also linearized, as depicted in Fig. 16(a), with ACPR of −51.71/−50.22 dBc.

3) Beam-Oriented DPD for 1×4 ULA: The spectral results of PA reconstruction are demonstrated in Fig. 17(a). Estimated outputs of four PAs agree with the actual output of four PAs, where NMSEs are −34.37, −35.77, −39.41, and −38.76 dB.

TABLE VII

MEASURED PERFORMANCE OF THE PROPOSED METHOD WITH FULL-ANGLE DPD

	NMSE (dB)			ACPR (dBc)		
	PA1	PA2	Main Beam	PA1	PA2	Main Beam
w/o DPD	-25.95	-25.64	-26.44	-37.28/ -36.23	-36.29/ -35.76	-37.12/ -36.48
w/ DPD	-38.46	-37.53	-41.14	-49.30/ -47.77	-47.93/ -46.83	-51.71/ -50.22

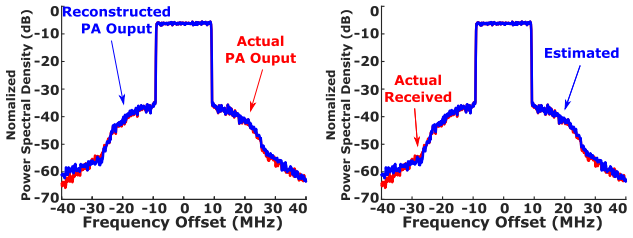

(a) (b)

Fig. 17. Measurement results of signal reconstruction with beam-oriented DPD in 1 × 4 ULA. (a) Fourth PA. (b) Far-field main beam signals.

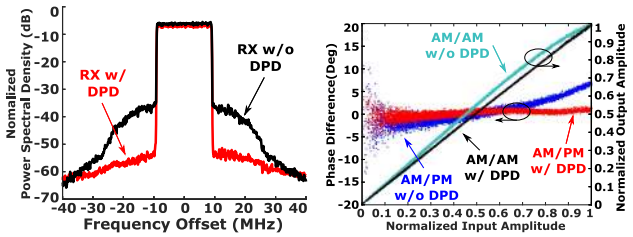

(a) (b)

Fig. 18. Measured linearization performance on far-field signals with beam-oriented DPD in 1 × 4 ULA. (a) Spectrum comparison. (b) AM–AM and AM–PM results.

Fig. 17(b) shows good agreement between the estimated and actual far-field main beam signals with NMSE of −41.36 dB. Fig. 18 shows the linearization performance of the proposed MIMO DPD method with ACPR of −49.98/−47.88 dBc.

VI. CONCLUSION

In this article, a novel DPD architecture with real-time OTA data acquisition for massive MIMO transmitter has been proposed. A single OTA receiver is employed to capture data for indirect PA identification by taking advantage of the beam-steering scenario. According to the simulation and experimental validation, the proposed method can accurately predict the PA output signals and efficiently linearize the mmWave MIMO transmitters with low complexity, proving itself as a viable solution to the linearization of 5G massive MIMO transmitters.

It is worth noting that although only a single user linear array case was demonstrated in the article and a small number of RF chains were used in the experimental test due to limitation of available facility in the lab, the principle of the proposed approach is generally extendable and it can be easily applied to other types of arrays and more complicated

multiuser MIMO communication systems. The proposed DPD method is solely based on the assumption that the far-field signals are the linear combinations of the transmitted signals from the RF chains, which is valid in not only linear arrays but also the other types of arrays, such as 2-D arrays. For instance, moving from linear array to 2-D array, we just need to change the radiation angle α in (2) to 2-D. The generalization to multiuser MIMO systems is also possible. For example, in the popular hybrid MIMO system where each user transmits the signal via a separate subarray, the proposed method can be directly applied by processing each subarray one by one. Furthermore, for proof of concept, in this article, some practical effects, e.g., the physical configuration of the antennas and attenuation of the channel, are omitted. Although the actual linearization performance may vary, these effects do not impact the operation principle of the proposed approach.

APPENDIX
DERIVATION OF $\mathbb{E}\boldsymbol{\Delta}$

The expectation of $\boldsymbol{\Delta}$ can be derived as follows. $\boldsymbol{\Delta}$ is the solution to (26). Each row of $\boldsymbol{\Delta}$ can be solved independently, so without loss of generality, we solve the kth row of $\boldsymbol{\Delta}$, i.e., $\boldsymbol{\Delta}_{\mathbf{k}}$. The linear system to be solved becomes

$$\boldsymbol{\Delta}_{\mathbf{k}}\boldsymbol{\Psi}_{\boldsymbol{\beta}} = \mathbf{H}_{\mathbf{k}} \tag{A.1}$$

where

$$\mathbf{H}_{\mathbf{k}} = \left[\sum_{n=1}^{N} h_{nk}e^{j(k-1)\beta_1+j(n-1)\theta}, \ldots, \sum_{n=1}^{N} h_{nk}e^{j(k-1)\beta_M+j(n-1)\theta}\right]. \tag{A.2}$$

Therefore, the correlation between the pth row of $\boldsymbol{\Psi}_{\boldsymbol{\beta}}$, i.e., $\boldsymbol{\Psi}_{\mathbf{p}}$, and $\mathbf{H}_{\mathbf{k}}$ is

$$\begin{aligned}\mathrm{Corr}_k^{(p)} &= \sum_{m=1}^{M} \mathbf{H}_{\mathbf{k}}(m)\overline{\boldsymbol{\Psi}_{\mathbf{p}}(m)} \\ &= \sum_{m=1}^{M}\left(\sum_{n=1}^{N} h_{nk}e^{j[(k-1)\beta_m+(n-1)\theta]}\right)e^{-j(p-1)(\beta_m+\theta)} \\ &= \sum_{m=1}^{M}\sum_{n=1}^{N} h_{nk}e^{j[(k-p)\beta_m+(n-p)\theta]} \\ &= \sum_{n=1}^{N} h_{nk}e^{j(n-p)\theta}\sum_{m=1}^{M} e^{j(k-p)\beta_m}. \end{aligned} \tag{A.3}$$

Thus

$$\begin{aligned}\mathbb{E}\,\mathrm{Corr}_k^{(p)} &= \mathbb{E}\sum_{n=1}^{N} h_{nk}e^{j(n-p)\theta}\sum_{m=1}^{M} e^{j(k-p)\beta_m} \\ &= \sum_{n=1}^{N} h_{nk}e^{j(n-p)\theta}\sum_{m=1}^{M}\mathbb{E}\,e^{j(k-p)\beta_m}. \end{aligned} \tag{A.4}$$

Since the movement of users can be considered to be random, we consider β_m to obey uniform distribution within the range $[0, 2\pi]$. Thus, we have

$$\mathbb{E}\,e^{j(k-p)\beta_m} = \begin{cases} 0, & k \neq p \\ 1, & k = p. \end{cases} \tag{A.5}$$

Therefore

$$\mathbb{E}\,\mathrm{Corr}_k^{(p)} = \begin{cases} 0, & k \neq p \\ M\sum_{n=1}^{N} h_{nk}e^{j(n-p)\theta}, & k = p. \end{cases} \tag{A.6}$$

Since only one row in $\boldsymbol{\Psi}$ has nonzero correlation with $\mathbf{H}_{\mathbf{k}}$, $\mathbb{E}\,\boldsymbol{\Delta}_{\mathbf{k}}$ will only have one nonzero element.

As $\mathbb{E}\,\boldsymbol{\Psi}\boldsymbol{\Psi}^H = M\mathbf{I}$, $\mathbb{E}\boldsymbol{\Delta}$ can be solved to be

$$\mathbb{E}\boldsymbol{\Delta} = \begin{bmatrix} \sum_{n=1}^{N} h_{n1}e^{j(n-1)\theta} & 0 & \cdots \\ 0 & \sum_{n=1}^{N} h_{n2}e^{j(n-2)\theta} & \cdots \\ \vdots & \vdots & \ddots \end{bmatrix}. \tag{A.7}$$

All off-diagonal elements are zero, and the diagonal elements only depend on the coupling coefficients and the direction of DPD receiver.

REFERENCES

[1] S. Mumtaz, J. Rodriguez, and L. Dai, *mmWave Massive MIMO: A Paradigm for 5G*. New York, NY, USA: Academic, 2016.

[2] L. Guan and A. Zhu, "Green communications: Digital predistortion for wideband RF power amplifiers," *IEEE Microw. Mag.*, vol. 15, no. 7, pp. 84–99, Nov./Dec. 2014.

[3] F. M. Ghannouchi and O. Hammi, "Behavioral modeling and predistortion," *IEEE Microw. Mag.*, vol. 10, no. 7, pp. 52–64, Dec. 2009.

[4] C. Fager, T. Eriksson, F. Barradas, K. Hausmair, T. Cunha, and J. C. Pedro, "Linearity and efficiency in 5G transmitters: New techniques for analyzing efficiency, linearity, and linearization in a 5G active antenna transmitter context," *IEEE Microw. Mag.*, vol. 20, no. 5, pp. 35–49, May 2019.

[5] S. A. Bassam, M. Helaoui, and F. M. Ghannouchi, "Crossover digital predistorter for the compensation of crosstalk and nonlinearity in MIMO transmitters," *IEEE Trans. Microw. Theory Techn.*, vol. 57, no. 5, pp. 1119–1128, May 2009.

[6] A. Abdelhafiz, L. Behjat, F. M. Ghannouchi, M. Helaoui, and O. Hammi, "A high-performance complexity reduced behavioral model and digital predistorter for MIMO systems with crosstalk," *IEEE Trans. Commun.*, vol. 64, no. 5, pp. 1996–2004, May 2016.

[7] S. Amin, P. Landin, P. Händel, and D. Rönnow, "Behavioral modeling and linearization of crosstalk and memory effects in RF MIMO transmitters," *IEEE Trans. Microw. Theory Techn.*, vol. 62, no. 4, pp. 810–823, Apr. 2014.

[8] K. Hausmair, P. N. Landin, U. Gustavsson, C. Fager, and T. Eriksson, "Digital predistortion for multi-antenna transmitters affected by antenna crosstalk," *IEEE Trans. Microw. Theory Techn.*, vol. 66, no. 3, pp. 1524–1535, Mar. 2018.

[9] F. M. Barradas, T. R. Cunha, and J. C. Pedro, "Digital predistortion of RF PAs for MIMO transmitters based on the equivalent load," in *Proc. Integr. Nonlinear Microw. Millim.-Wave Circuits Workshop (INMMiC)*, Apr. 2017, pp. 1–4.

[10] S. K. Dhar, A. Abdelhafiz, M. Aziz, M. Helaoui, and F. M. Ghannouchi, "A reflection-aware unified modeling and linearization approach for power amplifier under mismatch and mutual coupling," *IEEE Trans. Microw. Theory Techn.*, vol. 66, no. 9, pp. 4147–4157, Sep. 2018.

[11] S. Lee *et al.*, "Digital predistortion for power amplifiers in hybrid MIMO systems with antenna subarrays," in *Proc. IEEE 81st Veh. Technol. Conf. (VTC Spring)*, May 2015, pp. 1–5.

[12] N. Tervo, J. Aikio, T. Tuovinen, T. Rahkonen, and A. Parssinen, "Digital predistortion of amplitude varying phased array utilising over-the-air combining," in *IEEE MTT-S Int. Microw. Symp. Dig.*, Jun. 2017, pp. 1165–1168.

[13] X. Liu *et al.*, "Beam-oriented digital predistortion for 5G massive MIMO hybrid beamforming transmitters," *IEEE Trans. Microw. Theory Techn.*, vol. 66, no. 7, pp. 3419–3432, Jul. 2018.
[14] M. Abdelaziz, L. Antilla, A. Brihuega, F. Tufvesson, and M. Valkama, "Digital predistortion for hybrid MIMO transmitters," *IEEE J. Sel. Topics Signal Process.*, vol. 12, no. 3, pp. 445–454, Jun. 2018.
[15] S. Choi and E.-R. Jeong, "Digital predistortion based on combined feedback in MIMO transmitters," *IEEE Commun. Lett.*, vol. 16, no. 10, pp. 1572–1575, Oct. 2012.
[16] L. Liu, W. Chen, L. Ma, and H. Sun, "Single-PA-feedback digital predistortion for beamforming MIMO transmitter," in *Proc. IEEE Int. Conf. Microw. Millim. Wave Technol. (ICMMT)*, vol. 2, Jun. 2016, pp. 573–575.
[17] K. Hausmair, U. Gustavsson, C. Fager, and T. Eriksson, "Modeling and linearization of multi-antenna transmitters using over-the-air measurements," in *Proc. IEEE Int. Symp. Circuits Syst. (ISCAS)*, May 2018, pp. 1–4.
[18] Q. Luo, C. Yu, and X.-W. Zhu, "Digital predistortion of phased array transmitters with multi-channel time delay," in *Proc. IEEE Topical Conf. RF/Microw. Power Amplif. Radio Wireless Appl. (PAWR)*, Jan. 2018, pp. 54–57.
[19] H. T. Dabag, B. Hanafi, O. D. Gürbüz, G. M. Rebeiz, J. F. Buckwalter, and P. M. Asbeck, "Transmission of signals with complex constellations using millimeter-wave spatially power-combined CMOS power amplifiers and digital predistortion," *IEEE Trans. Microw. Theory Techn.*, vol. 63, no. 7, pp. 2364–2374, Jul. 2015.
[20] X. Wang, C. Yu, Y. Li, W. Hong, and A. Zhu, "Real-time single channel over-the-air data acquisition for digital predistortion of 5G massive MIMO wireless transmitters," in *IEEE MTT-S Int. Microw. Symp. Dig.*, May 2019, pp. 1–3.
[21] C. Yu *et al.*, "Full-angle digital predistortion of 5G millimeter-wave massive MIMO transmitters," *IEEE Trans. Microw. Theory Techn.*, vol. 67, no. 7, pp. 2847–2860, Jul. 2019.
[22] H. Kong, Z. Wen, Y. Jing, and M. Yau, "Midfield over-the-air test: A new OTA RF performance test method for 5G massive MIMO devices," *IEEE Trans. Microw. Theory Techn.*, vol. 67, no. 7, pp. 2873–2883, Jul. 2019.
[23] L. Ding *et al.*, "A robust digital baseband predistorter constructed using memory polynomials," *IEEE Trans. Commun.*, vol. 52, no. 1, pp. 159–165, Jan. 2004.
[24] Y. Li, W. Cao, and A. Zhu, "Instantaneous sample indexed magnitude-selective affine function-based behavioral model for digital predistortion of RF power amplifiers," *IEEE Trans. Microw. Theory Techn.*, vol. 66, no. 11, pp. 5000–5010, Nov. 2018.
[25] P. Gröschel *et al.*, "A system concept for online calibration of massive MIMO transceiver arrays for communication and localization," *IEEE Trans. Microw. Theory Techn.*, vol. 65, no. 5, pp. 1735–1750, May 2017.

Xiaoyu Wang (S'18) received the B.E. degree in information engineering from Southeast University, Nanjing, China, in 2015. She is currently pursuing the Ph.D. degree at University College Dublin (UCD), Dublin, Ireland.

She is currently with the RF and Microwave Research Group, UCD. Her current research interests include digital predistortion for RF power amplifiers, with a particular emphasis on applications to multiple-input–multiple-output (MIMO) systems.

Yue Li (S'17) received the B.E. degree in information engineering from Southeast University, Nanjing, China, in 2016. He is currently pursuing the Ph.D. degree at University College Dublin (UCD), Dublin, Ireland.

He is currently with the RF and Microwave Research Group, UCD. His current research interests include behavioral modeling and digital predistortion for RF power amplifiers.

Chao Yu (S'09–M'15) received the B.E. degree in information engineering and the M.E. degree in electromagnetic fields and microwave technology from Southeast University (SEU), Nanjing, China, in 2007 and 2010, respectively, and the Ph.D. degree in electronic engineering from University College Dublin (UCD), Dublin, Ireland, in 2014.

He is currently an Associate Professor with the State Key Laboratory of Millimeter Waves, School of Information Science and Engineering, SEU, and Purple Mountain Laboratories, Nanjing. His current research interests include microwave and millimeter-wave power amplifier modeling and linearization and 5G massive multiple-input–multiple-output (MIMO) RF system design.

Wei Hong (M'92–SM'07–F'12) received the B.S. degree from the University of Information Engineering, Zhengzhou, China, in 1982, and the M.S. and Ph.D. degrees from Southeast University, Nanjing, China, in 1985 and 1988, respectively, all in radio engineering.

Since 1988, he has been with the State Key Laboratory of Millimeter Waves, where he has been serving as the Director since 2003 and is currently a Professor and the Dean of the School of Information Science and Engineering, Southeast University. In 1993 and from 1995 to 1998, he was a short-term Visiting Scholar with the University of California at Berkeley, Berkeley, CA, USA, and the University of California at Santa Cruz, Santa Cruz, CA, USA, respectively. He has been engaged in numerical methods for electromagnetic problems, millimeter-wave theory and technology, antennas, RF technology for wireless communications, and so on. He has authored or coauthored over 300 technical publications with over 9000 citations and authored two books.

Dr. Hong is also a Fellow of CIE and the Vice President of the CIE Microwave Society and Antenna Society. He was twice awarded the National Natural Prizes, thrice awarded the first-class Science and Technology Progress Prizes issued by the Ministry of Education of China and Jiangsu Province Government, and so on. He also received the Foundations for China Distinguished Young Investigators and for "Innovation Group" issued by NSF of China. He is also the Chair of the IEEE MTT-S/AP-S/EMC-S Joint Nanjing Chapter and was an elected IEEE MTT-S AdCom Member from 2014 to 2016. He has served as an Associate Editor for the IEEE TRANSACTIONS ON MICROWAVE THEORY AND TECHNIQUES from 2007 to 2010. He was one of the Guest Editors for the 5G Special Issue of the IEEE TRANSACTIONS ON ANTENNAS AND PROPAGATION in 2017.

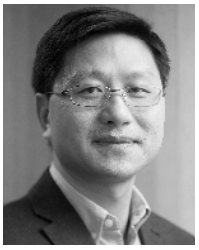

Anding Zhu (S'00–M'04–SM'12) received the Ph.D. degree in electronic engineering from University College Dublin (UCD), Dublin, Ireland, in 2004.

He is currently a Professor with the School of Electrical and Electronic Engineering, UCD. His current research interests include high-frequency nonlinear system modeling and device characterization techniques, high-efficiency power amplifier design, wireless transmitter architectures, digital signal processing, and nonlinear system identification algorithms. He has published more than 120 peer-reviewed journal and conference articles.

Prof. Zhu is an elected member of MTT-S AdCom, the Vice Chair of the Publications Committee, and the Vice Chair of the Electronic Information Committee. He served as the Secretary of MTT-S AdCom in 2018. He was the General Chair of the 2018 IEEE MTT-S International Microwave Workshop Series on 5G Hardware and System Technologies (IMWS-5G) and a Guest Editor of the IEEE TRANSACTIONS ON MICROWAVE THEORY AND TECHNIQUES on 5G Hardware and System Technologies. He is also the Chair of the MTT-S Microwave High-Power Techniques Committee and an Associate Editor of the *IEEE Microwave Magazine*.